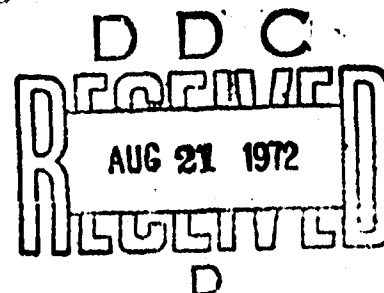AD

AD 746955

# THE EFFECT OF AGING TIME

# ON SPALLATION OF

# 2024-T6 ALUMINUM

ROBERT B. HERRING and GREGORY B. OLSON

METALS DIVISION

December 1971

Approved for public release; distribution unlimited.

D D C

AUG 21 1972

D

ARMY MATERIALS AND MECHANICS RESEARCH CENTER
Watertown, Massachusetts 02172

## DOCUMENT CONTROL DATA - R & D

*(Security classification of title, body of abstract and indexing annotation must be entered when the overall report is classified)*

| 1. ORIGINATING ACTIVITY (Corporate author) | 2a. REPORT SECURITY CLASSIFICATION |
|---|---|
| Army Materials and Mechanics Research Center<br>Watertown, Massachusetts  02172 | Unclassified |
| | 2b. GROUP |

**3. REPORT TITLE**

THE EFFECT OF AGING TIME ON SPALLATION OF 2024-T6 ALUMINUM

**4. DESCRIPTIVE NOTES** *(Type of report and inclusive dates)*

**5. AUTHOR(S)** *(First name, middle initial, last name)*

Robert B. Herring and Gregory B. Olson

| 6. REPORT DATE | 7a. TOTAL NO. OF PAGES | 7b. NO. OF REFS |
|---|---|---|
| December 1971 | 33 | 19 |

| 8a. CONTRACT OR GRANT NO. | 9a. ORIGINATOR'S REPORT NUMBER(S) |
|---|---|
| b. PROJECT NO. D/A 1B062113A661 | AMMRC TR 71-61 |
| c. AMCMS Code Number 502N.11.07000 | 9b. OTHER REPORT NO(S) *(Any other numbers that may be assigned this report)* |
| d. Agency Accession Number DA 0B4811 | |

**10. DISTRIBUTION STATEMENT**

Approved for public release; distribution unlimited.

| 11. SUPPLEMENTARY NOTES | 12. SPONSORING MILITARY ACTIVITY |
|---|---|
| | U.S. Army Materiel Command<br>Washington, D.C.  20315 |

**13. ABSTRACT**

Incipient spall thresholds have been measured and spall fracture surfaces and internal structure examined for 2024 aluminum subjected to impulsive loading by a capacitance discharge flyer plate technique. The incipient spall threshold was found to be 10 to 15% higher in under peak hardness material compared to that aged to peak hardness or overaged. The spall fracture surfaces in the underaged specimens also showed the greatest effect of the high strain rate loading. In that condition, the very ductile fracture mode, observed at low rates, was changed to a less ductile appearing fracture mode dominated by the presence of inclusions. The work hardening ability of the various aged conditions, as determined from low rate tensile tests, was found to correlate with the ability of those conditions to show shock hardening and with the retention of dislocations in the structure following the high rate loading. (Authors)

DD FORM 1473 REPLACES DD FORM 1473, 1 JAN 64, WHICH IS OBSOLETE FOR ARMY USE.

UNCLASSIFIED
Security Classification

| 14 KEY WORDS | LINK A | | LINK B | | LINK C | |
|---|---|---|---|---|---|---|
| | ROLE | WT | ROLE | WT | ROLE | WT |
| Aluminum alloys | | | | | | |
| Stress waves | | | | | | |
| Impact tests | | | | | | |
| Dynamic tests | | | | | | |
| Spalling | | | | | | |
| Fracture | | | | | | |
| Fractography | | | | | | |

AMMRC TR 71-61

# THE EFFECT OF AGING TIME ON SPALLATION OF 2024-T6 ALUMINUM

Technical Report by

*ROBERT B. HERRING and GREGORY B. OLSON\**

December 1971

METALS DIVISION
ARMY MATERIALS AND MECHANICS RESEARCH CENTER
Watertown, Massachusetts 02172

\*Graduate Student, Department of Metallurgy, Massachusetts Institute of Technology, Cambridge, Massachusetts.

CONTENTS

## INTRODUCTION

If sheet material is subjected to a plane compressive load of short dura-
tion, a plane compressive stress wave is generated which propagates through
the thickness of the material. When the loading wave reaches the rear free
surface, a relief wave is generated which propagates back into the material.
At the point where that reflection relief wave reaches the relief wave forming
the end of the load pulse, they superimpose and, internally, the material is
subjected to a tensile stress state. The result can be a fracture mode,
called spallation, in which internal separation of the material develops as a
result of the stress wave reflections and interactions.

However, in ductile materials, spallation does not occur as an instanta-
neous process but by cumulative processes which depend on the stress level and
duration of the stress. Thus, the material may sustain quite high tensile
stresses provided their time of application at any given point in the material
is very short. The stress levels and pulse durations to produce some specified
level of damage in a material define the spall threshold for that material.
Careful usage reserves the term "spall" for the process resulting in actual
material separation due to stress wave effects, while the term "incipient spall"
is used to denote the process leading to internal separations in the material,
short of actual separation.

Although the spall and incipient spall threshold values have been
measured for a variety of materials,[1-4]  very little is known of the ways in
which material properties influence that threshold or of the role of micro-
structural constituents in the initiation or propagation of spall fractures.
In particular, no previous study is known in which an attempt has been made to
study the effect of the precipitation state of an age hardenable material on
the spall threshold.

For this study, a commercial 2024 aluminum alloy was prepared in three
aged conditions and subjected to impulsive loading using an exploding foil
flyer plate technique. One specimen set was aged to less than peak hardness,
one set was aged to peak hardness, and one set was overaged. The impulsively
loaded specimens were recovered and studied by optical metallographic, scan-
ning and transmission electron microscopy techniques in addition to micro-
hardness tests. Uniaxial tensile tests were carried out on similar material,
and those results have been used in interpreting differences in the spallation
behavior of the three conditions of the aluminum alloy.

# EXPERIMENTAL PROCEDURE

## I.   Materials

The material used for this study was a commercial 2024, age hardenable, aluminum alloy containing nominally 4.5% Cu, 1.5% Mg, and 0.6% Mn by weight. The material was received in the form of 5/8-inch-thick plate in the T351 (cold rolled) condition.

The age hardening of the material was followed by solution treating several cubes of the material at 497C for three hours, quenching into cold water, and aging in an air furnace at 190C. During the aging, hardness changes were followed by measurements made on a Wilson Rockwell hard..ess tester using the F scale. Figure 1 shows the hardness as a function of aging time at 190C for this material. The peak hardness was attained at about 12 hours aging time. Accepted heat treating practice for the T6 (artificially aged) condition for this alloy is solution treatment at between 488C and 499C followed by aging at 185C to 196C for 11 to 13 hours for attainment of peak hardness.[5]

The data shown in Figure 1 was used in selecting conditions of 1, 12, and 100 hours at 190C to produce the three conditions of underaged, peak hardness, and overaged structures in the alloy for the spall experiments.
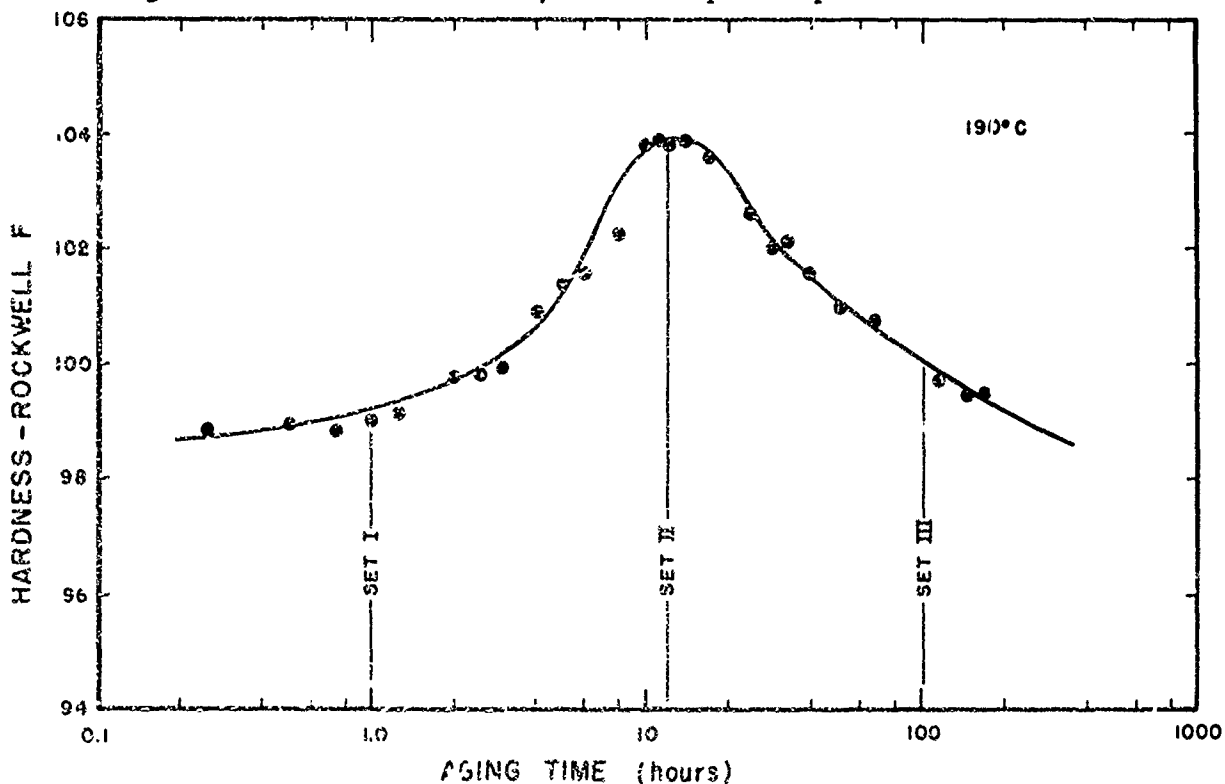


Figure 1.  Hardness Versus Aging Time for 2024 Aluminum Quenched from 497C and Aged at 190C

## II. Shock Loading

Specimens for shock loading were prepared by machining 2.0-by 2.0-by 0.250-inch blanks from the center of the 5/8-inch plate. Those blanks were solution treated for three hours at 497 ± 2C and quenched into cold water with agitation. Aging was performed in a circulating air furnace at 190 ± 1C for 1, 12, and 100 hours for specimen sets I, II, and III respectively. After aging, the surfaces of the specimen blanks were lightly polished on metallographic paper to remove the oxide layer formed during the heat treatment.

Six blanks of each of the three conditions were sent to the Physics Division of the Air Force Materials Laboratory, Wright-Patterson AFB, Ohio, for impulsive loading. The impulsive loading was carried out at AFML by personnel of the Dayton Research Institute. Testing of this 2024 aluminum was combined with their program testing of 7075 aluminum material. A summary of the conditions used for the impulsive loading is included in the Appendix.

For impulsive loading, the largest specimen which could be accommodated in the test facility was 1.4 inches square. Accordingly, four of the 2.0 inch squares were cut down to 1.4 inches square and the other two were quartered. This provided 12 specimens of each of the three material conditions as follows: four specimens 1.4 inches square and eight specimens approximately 1.0 inch square.

The specimens were mounted for testing by low acoustical impedance rubber adhesive applied along two edges with the other edges free (the "free surface" support system of the Appendix). The impacted surface was 0.5 inch above a 0.5-mil-thick aluminum foil which was covered by a 5-mil mylar film. The specimen region was enclosed by a vacuum chamber approximately six inches high which was evacuated to 5 to 80 torr by a mechanical pump prior to a test. The vacuum chamber was sealed at the top by a thin plastic film.

When high voltage from a capacitor bank was applied to the aluminum foil, the foil was vaporized, accelerating the 1.5-inch-square mylar flyer plate toward the specimen. Travel of that mylar flyer plate was photographed by a Beckman model 300 framing camera. The velocity and planarity of impact of the flyer plate, shown in the Appendix, were determined from the framing camera record. The velocity measurements were computed by a least squares fit to position data taken from six or more frames.

When the flyer plate impacted the specimen, momentum was imparted to it, and the specimen flew upward tearing out the thin plastic film sealing the top of the vacuum chamber. The specimen was brought to rest in a padded recovery chamber and recovered for later study.

When the flyer plate impacts a specimen, a compressive stress wave is created which propagates in the specimen and, also, a wave propagates back into the flyer plate. The length of the loading pulse is determined by the time required for the wave to pass through the flyer plate to the free back surface and for a relief wave to return to the impacting surface.

The longitudinal sound velocity in the 2024 aluminum was measured to be 6.44 mm/μsec (see the Appendix). The sonic velocity of the mylar flyer plate is 2.2 mm/μsec.[6]  Hence, the time required for a pulse to traverse the 5-mil mylar flyer plate and the relief wave return would be about 0.15 μsec (neglecting the correction for the change of properties with pressure). The loading pulse of 0.15-μsec duration would then occupy a length of about 0.96 mm (0.039 inch) as it travels in the aluminum.

The details of the techniques of exploding foil flyer plate testing have been described in the literature[7,8]   and will not be reviewed here.

It would have been desirable to obtain back surface velocity measurements on the specimens as the stress wave was propagated through them. From those measurements of wave profiles, the attenuation characteristics of the material could have been determined. However, equipment to make such measurements was not available at AFML.

III. Optical Microscopy and Microhardness Measurements

Specimens from the three sets of material were sectioned by spark cutting. They were mounted and polished for metallographic study. In mounting the specimens, the incipient spall cracks were vacuum impregnated by a resin base material to retain the edge detail of the cracks. For comparative purposes, a set of sectioned specimens was selected which represents examples from the three types of material at relatively well matched impact velocities of 1.3, 1.8, 2.3, and 2.5 mm/μsec.

Microhardness measurements were taken using a Vickers pyramidal diamond indenter and using a 100-gram load at approximately a 0.015-inch spacing across the 0.25 inch thickness of the sectioned specimens.

IV. Scanning Electron Microscopy of Fracture Surfaces

The rolling of the original plate produced a grain orientation effect not completely removed by the solution treatment. Therefore, for comparison purposes, slow rate tensile fractures in the short transverse orientation were obtained and compared with the fracture surfaces produced in the spall fractures. Tensile specimens were prepared which were approximately 0.050 by 0.050 by 0.250 inches by spark cutting specimens out of the thickness of un-shocked material subjected to the same heat treatment as the impact specimens. The tensile specimens were notched on one side by a 0.005-inch spark cut and pulled at 0.02 in/min in an Instron testing machine. The incipient spall and slow tensile fracture surfaces from each set were examined and compared by scanning electron microscopy.

V.   Transmission Electron Microscopy

Sections 0.015 inch thick were cut normal to the plate surface from unshocked and shocked material in the three aged conditions. The slices were electropolished using a solution of 41.6 g $CrO_3$, 74.6 ml $H_2O$, 192 ml $H_3PO_4$, and

4

34.6 ml $H_2SO_4$ at 12 volts at 40C. [9] The standard "window" technique of thinning was used. After thinning, the specimens were rinsed in a cleaning solution[9] of 5 g $CrO_3$, 117 ml $H_2O$, and 4 ml $H_3PO_4$ at 40C followed by rinses in distilled water and ethyl alcohol. Examination was carried out on a Hitachi HU-11 microscope operated at 100 kV.

## VI. Uniaxial Tensile Tests

The spall fracture occurs almost parallel to the plane of the plate surface. Hence, the mechanical properties of greatest interest would be those in the short transverse direction through the plate thickness. However, due to problems of gripping specimens which could be no more than 5/8 inch long overall (the original plate thickness), the yield and ultimate stress values obtained on the short transverse fracture specimens, described above, were not sufficiently precise for use in characterizing the material properties. However, the short transverse properties can be expected to follow the trends of the properties measured in the plane of the sheet transverse to the rolling direction.

Tensile specimen blanks in the form of 3/8-inch cylinders, 2.5 inches long, were machined from the same stock as that used for the impulsive loading specimens. The specimen blanks were taken transverse to the rolling direction. They were solution treated at 497C for three hours and quenched in cold water. The blanks were then aged at 190C in a circulating air furnace for times of 0, 1, 9, 14, and 100 hours. After aging, the blanks were finished to tensile specimens having a 0.252 inch diameter in the 1.00 inch gauge section with 3/8-inch threaded grip ends (a modified TR-4 tensile specimen).

Tensile tests were conducted using a traveling diameter gauge developed in the Metals Division of AMMRC. [10] That gauge has sensing fingers which travel up and down the gauge length to detect necking of the specimen so that the diameter profile can be recorded along with the load curve. From measurements of the minimum diameter, true stress - true strain curves were plotted.

The work hardening coefficient, n, in the power relation

$$\sigma = K\epsilon^{n}$$

was determined from lines fitted to log-log plots of the true stress - true strain data. The 0.2% yield strength, $\sigma_y$, the ultimate tensile strength, $\sigma_{uts}$, strain to fracture, $\epsilon_f$, and the ratio of the ultimate to yield strength were also determined for each specimen.

RESULTS

## I. Surface Observations

The recovered shock loaded specimens were returned to AMMRC for study. The back surface of the specimens had raised blisters of varying size and severity which were the externally visible result of the incipient spall produced internally when the propagating stress wave reflected at the rear surface of the specimen. Figures 2, 3, and 4 show photographs of the back surface of the three sets of specimens. In these pictures, a light at a shallow angle to the surface was used to better reveal the raised blisters in the impacted specimens. The damage to the specimens impacted at the higher velocities is quite evident in the photographs and consisted in one case, in Figure 4, of complete separation of a layer of spalled material. Tables I, II, and III list the impact velocities and a visual assessment of damage for the specimens shown in Figures 2, 3, and 4.

### Table I - IMPACT VELOCITIES AND SURFACE DAMAGE ASSESSMENT - SET I

| Specimen No. | Shot No. | Velocity (mm/μsec) | Damage Observable at Surface |
|---|---|---|---|
| I-A | 5316* | 1.107 + 0.021 | No damage |
| I-B | 5315 | 1.241 + 0.020 | No damage |
| I-C | 5314 | 1.339 + 0.026 | No damage |
| I-D | 5313 | 1.806 + 0.046 | Light incipient spall |
| I-1 | 5305 | 1.7 + 0.1** | Very light incipient spall |
| I-2 | 5306 | 1.712 + 0.085 | Light incipient spall |
| I-3 | 5311 | 1.723 + 0.038 | Light incipient spall |
| I-4 | 5310 | 1.9 + 0.1** | Light incipient spall |
| I-5 | 5312 | 2.319 + 0.088 | Light incipient spall |
| I-6 | 5308 | 2.6 + 0.2** | Heavy 2/3 incipient spall |
| I-7 | 5307 | 2.672 + 0.057 | Light incipient spall |
| I-8 | 5309 | 2.986 + 0.053 | Heavy uniform incipient spall |

*Poor planarity of impact.
**Optical data insufficient to determine velocity.

6

Table II - IMPACT VELOCITIES AND SURFACE DAMAGE ASSESSMENT - SET II

| Specimen No. | Shot No. | Velocity (mm/μsec) | Damage Observed at Surface |
|---|---|---|---|
| II-A | 5332* | 0.467 + 0.011 | No damage |
| II-B | 5317 | 0.966 + 0.050 | No damage |
| II-C | 5333 | 1.174 + 0.059 | Very light incipient spall |
| II-D | 5331 | 1.953 + 0.063 | Very light incipient spall |
| II-1 | 5330 | 1.170 + 0.102 | No damage |
| II-2 | 5329 | 1.286 + 0.059 | Very light incipient spall |
| II-3 | 5328 | 1.5 + 0.1** | Very light incipient spall |
| II-4 | 5320 | 1.955 + 0.405 | Light incipient spall |
| II-5 | 5319 | 1.971 + 0.042 | Medium incipient spall |
| II-6 | 5321 | 2.189 + 0.021 | Medium incipient spall |
| II-7 | 5327 | 2.452 + 0.051 | Heavy 3/4 incipient spall |
| II-8 | 5322 | 2.841 + 0.153 | Heavy uniform incipient spall |

*Poor planarity of impact.
**Optical data insufficient to determine velocity.

Table III - IMPACT VELOCITIES AND SURFACE DAMAGE ASSESSMENT - SET III

| Specimen No. | Shot No. | Velocity (mm/μsec) | Damage Observed at Surface |
|---|---|---|---|
| III-A | 5340* | 0.690 + 0.021 | No damage |
| III-B | 5318* | 1.036 + 0.023 | No damage |
| III-C | 5339 | 1.292 + 0.041 | Very light incipient spall |
| III-D | 5338 | 1.859 + 0.044 | Light incipient spall |
| III-1 | 5326 | 1.374 + 0.035 | Very light incipient spall |
| III-2 | 5337 | 1.5 + 0.1** | Light incipient spall |
| III-3 | 5335 | 1.9 + 0.1** | Medium incipient spall |
| III-4 | 5336 | 1.992 + 0.126 | Medium incipient spall |
| III-5 | 5323 | 2.292 + 0.051 | Medium incipient spall |
| III-6 | 5325 | 2.491 + 0.042 | Heavy 4/5 incipient spall |
| III-7 | 5334 | 2.532 + 0.078 | Heavy uniform incipient spall |
| III-8 | 5324 | 2.650 + 0.072 | Heavy uniform spall |

*Poor planarity of impact.
**Optical data insufficient to determine velocity.
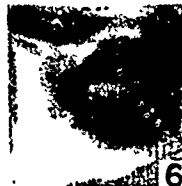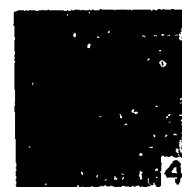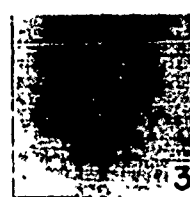
Figure 2. Set I - Back Surface Spall Damage Following Impulsive Loading
19-066-701/AMC-70

8
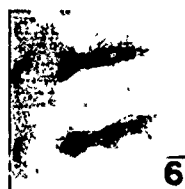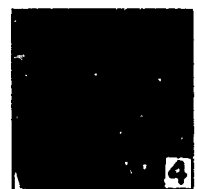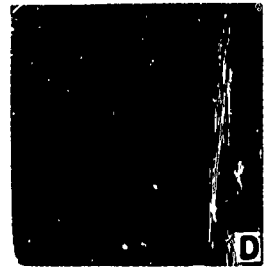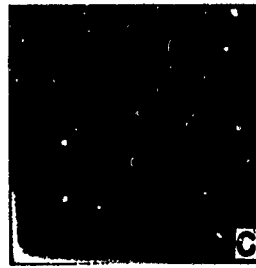
Figure 3. Set II - Back Surface Spall Damage Following Impulsive Loading
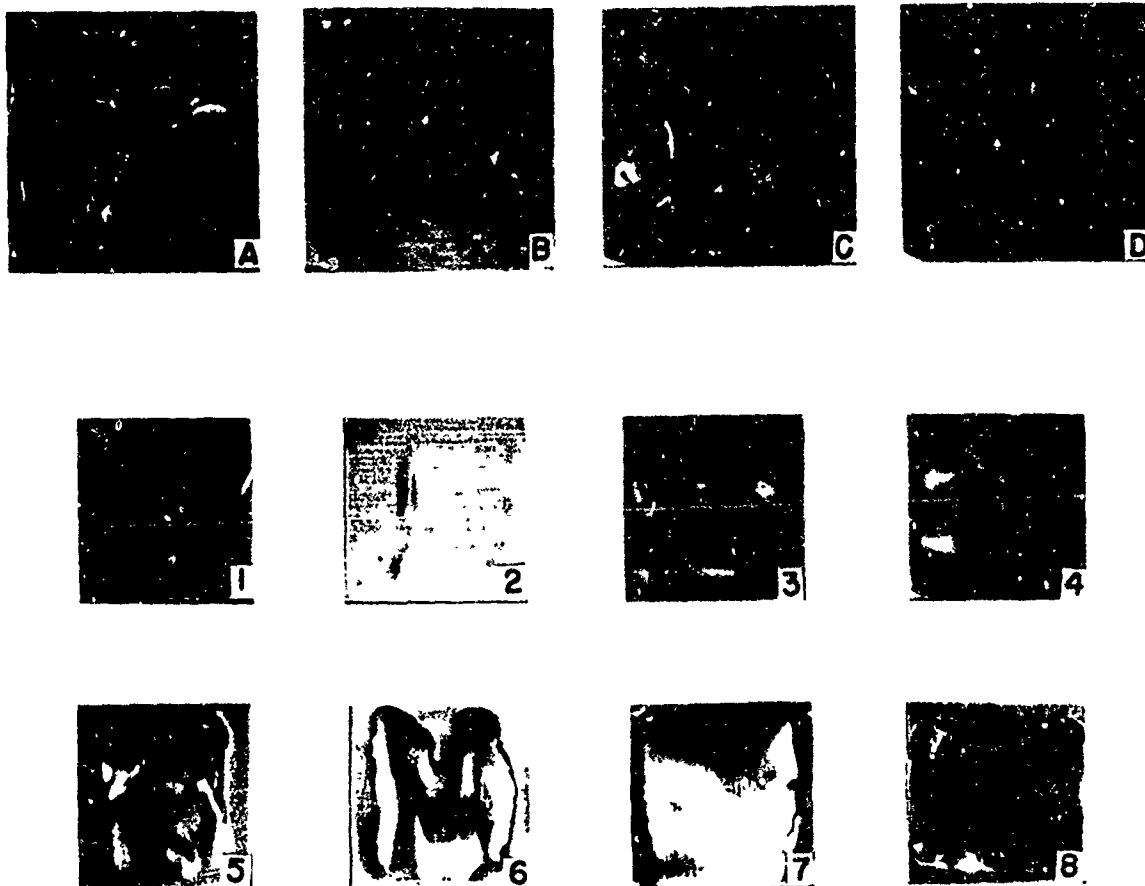19-066-700/AMC-70

9

Figure 4. Set III - Back Surface Spall Damage Following Impulsive Loading
19-066-699/AMC-70

10

In the photographs of the specimens, the top row (designated specimens A, B, C, and D) contains the four 1.4-inch-square specimens arranged from left to right in order of increasing impact velocity. The second and third rows of the photographs contain the eight smaller specimens (numbered 1 to 8) in order of increasing impact velocity for those eight specimens.

With the single exception of specimen I-6 of set I (shown in Figure 2), ordering the specimens according to impact velocity also orders them for increasing visually observable damage. The reported data for specimen I-6 (see Appendix) shows that the optical record for that test was poor but the impact velocity was estimated to be $2.6 \pm 0.2$ mm/$\mu$sec. The capacitor voltage on that shot was given as 18.07 kV and, in general, flyer plate velocity should be proportional to capacitor voltage. Based on the other velocity data and the capacitor voltage, the velocity should have been near 2.8 mm/$\mu$sec at the high end of the estimated range. If that higher impact velocity is accepted for specimen I-6, it should be interchanged with specimen I-7 in Figure 2; then for all specimens, surface evidence of incipient spall severity is directly related to impact velocity of the flyer plate.

Although it is difficult to define an incipient spall threshold from surface observation alone on only 12 specimens, the experienced personnel conducting the testing estimated the incipient spall threshold at 2200 to 2300 taps (1.27 to 1.33 mm/$\mu$sec) for set I material and at a lower value of 1800 to 2000 taps (1.04 to 1.15 mm/$\mu$sec) for the set II and set III materials (see Appendix). ("Taps" is a unit of impulse defined at 1 tap = 1 dyne-sec/cm$^2$ = $14.5 \times 10^{-6}$ lb-sec/in$^2$.) The incipient spall threshold was here defined as the lowest impact level which produced damage that was observable at the external surface. That observation was, however, confirmed by observations on sectioned specimens as described below.

II. Observations of Sectioned Specimens

A composite photograph showing central sections of specimens of the three material conditions at four impact levels is shown in Figure 5. From left to right across Figure 5, the internal incipient spall damage can be seen to increase with impact velocity. However, comparison among the sets of material shows certain differences which are believed to be due to the differing aging times. For example, comparison of the three samples at the lowest impact velocity shown in Figure 5 shows that some cracking is observable in the set II and set III material but not in specimen I-C of the set I material. Observation at higher magnifications confirmed that difference. Although specimen I-C did not show any propagating cracks, closer observation did reveal some cracked inclusion particles. Such cracked inclusions were not observed in unshocked material. The inclusions were probably intermetallics resulting from impurities introduced during casting of the original material.

Higher magnification study of the specimens shown in Figure 5 revealed several other features. Figure 6 shows the grain structure in the region of a spall crack in specimen I-D which was representative of all the specimens. In that figure, it can be seen that the incipient spall crack is made up of

SET I

I-C.  1.3 mm/μsec
I-D.  1.8 mm/μsec
I-5.  2.3 mm/μsec
I-6.  2.6 - 2.8 mm/μsec

I-C        I-D        I-5        I-6

SET II

II-1.  1.3 mm/μsec
II-C.  1.9 mm/μsec
II-6.  2.2 mm/μsec
II-7.  2.5 mm/μsec

II-1        II-C        II-6        II-7

SET III

III-C.  1.3 mm/μsec
III-D.  1.9 mm/μsec
III-5.  2.3 mm/μsec
III-7.  2.5 mm/μsec

III-C        III-D        III-5        III-7

Figure 5.  Composite Photo of Polished, Unetched Sections of Samples
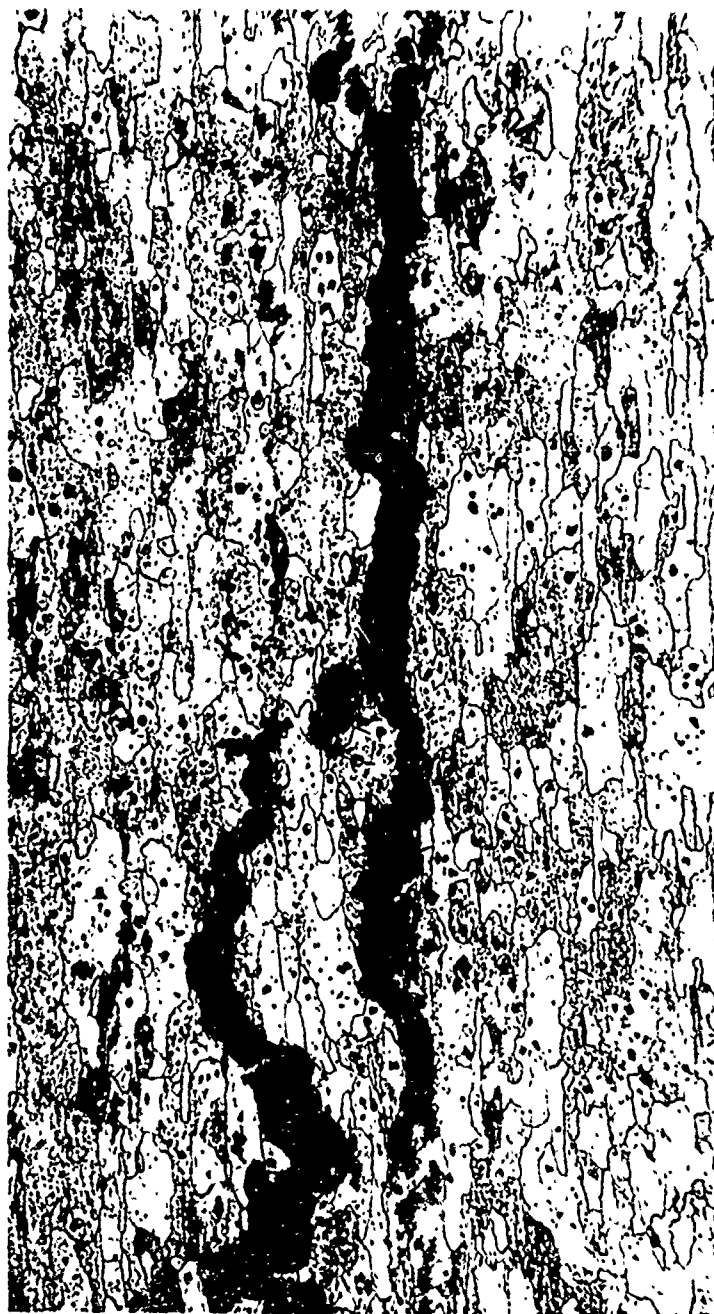Impacted at Comparable Flyer Plate Velocities (Impacted
from the Left) – 3X

Figure 6. Spall Crack at 100X in Specimen I-5 Impacted at 2.3 mm/μsec

a network of voids on several levels, roughly parallel to the specimen back surface, with the voids linked by shear cracks between the layers. Although a region of spall can be defined, a sharply defined spall plane was not present.

## III. Microhardness

Figure 7 is a plot for set I and set II of the change of hardness levels, $\Delta H$, in the impacted specimens compared to unshocked material across the 0.250-inch-thick specimen. Set I showed a large shock hardening effect while set II showed less hardening, and set III showed no detectable shock hardening. The incipient spall region location, near the backside of the specimens, is indicated on the figure.

From Figure 7, it is clear that the hardening was greatest near the impacted surface and increased with impact velocity. It was, however, some-what surprising that so little hardening occurred    the set III material.

## IV. Scanning Electron Microscopy

Figures 8 to 10 show scanning electron micrographs of typical areas of the spall, and slow tensile fracture surfaces of material from each set at magni-fications of 400X and 4000X. Comparison of the spall fractures (b and d of Figures 8 to 10) of the three sets shows that the influence of aging treatment on fracture mode is not great. The high magnification pictures suggest that the set I spall fracture (Figure 8d) is slightly less ductile; there are fewer fine cusps surrounding the inclusion particles. All the spall fracture sur-faces are dominated by those particles. Comparison with the slow tensile fractures (a and c of Figures 8 to 10) reveals little influence of strain rate on fracture appearance in the set II and set III material. The set I material, however, shows a pronounced strain rate effect. This effect is largely reflected in the much more ductile appearance of the slow tensile fracture as compared with any of the other fracture surfaces. The fracture is more like a classical ductile fracture by coalescence of voids, showing well rounded voids and many fine cusps. The surface is not dominated by the "chunky" inclusions which dominate the other surfaces.

## V. Transmission Studies

The material contained three types of particles. The largest, such as the one shown in Figure 11, were ellipsoidal, noncoherent particles, five to fifteen $\mu$ long and one to three $\mu$ thick, and elongated in the plate rolling direction. Particles of this type were widely distributed in the transmission foils at spacings estimated to be in the range of 500 to 1000$\mu$. By comparison with previous studies of 2024 aluminum[11]   it is believed those larger particles are Fe-Si intermetallic inclusions probably introduced into the ingot during casting.

A second class of noncoherent particles, such as those shown in Figure 12, was also present. Those particules were smaller, $0.5\mu$ to $1.0\mu$ long and 0.1 to $0.2\mu$ thick, and they were also elongated in the original plate rolling direction. They were rather uniformly distributed at particle spacings of
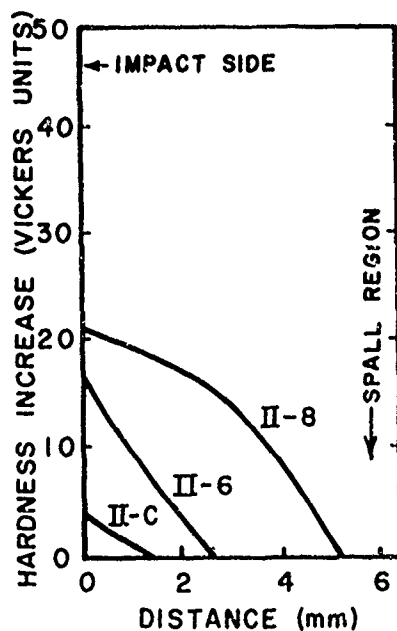
14
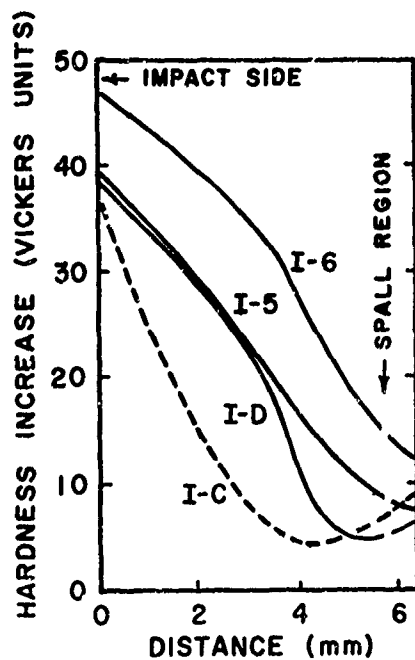
SET I

| SPECIMEN<br>No. | FLYER VELOCITY<br>(mm/$\mu$ sec) |
|---|---|
| I-6 | 2.6 |
| I-5 | 2.3 |
| I-D | 1.8 |
| I-C | 1.3 |

PRIOR TO IMPULSIVE LOADING
HARDNESS = 140 VPH

a

SET II

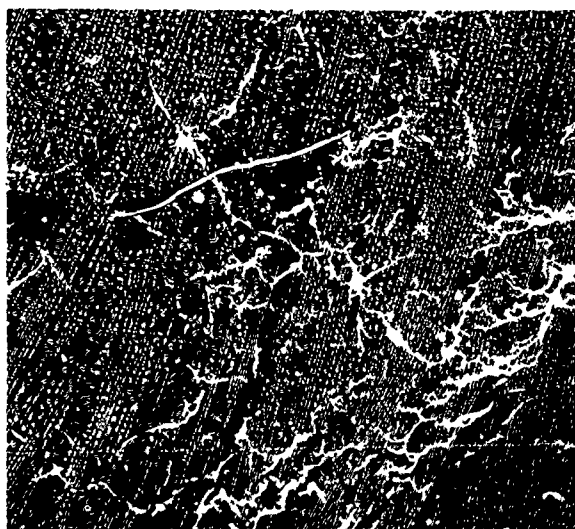| SPECIMEN<br>No. | FLYER VELOCITY<br>(mm/$\mu$ sec) |
|---|---|
| II-7 | 2.5 |
| II-6 | 2.2 |
| II-C | 1.9 |
| II-1 | 1.3 |
| (II-1 no effect) | |

PRIOR TO IMPULSIVE LOADING
HARDNESS = 158 VPH
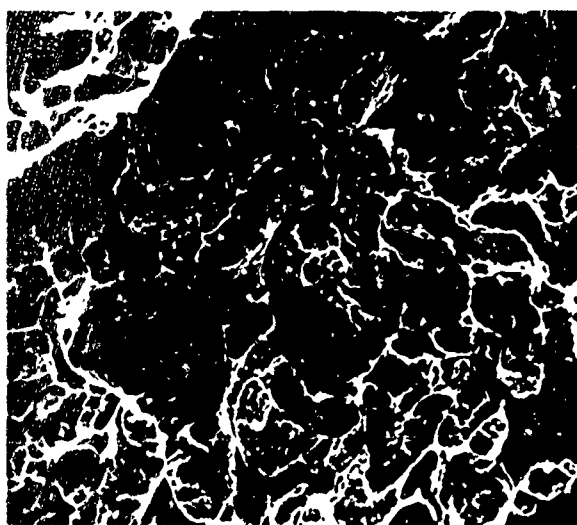
b

Figure 7. Shock Hardening Observed from Hardness Traverses on
Sectioned Specimens Shown in Figure 5
a) Set I
b) Set II

15
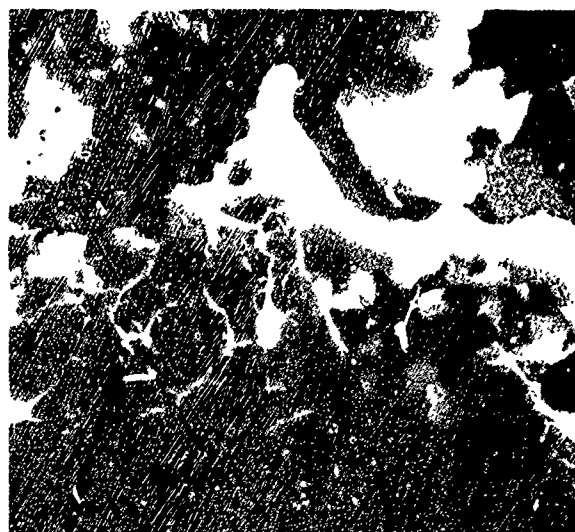
Figure 8. Scanning Electron Microscope Pictures of Fracture Surfaces
of Set I Material — Aged 1 Hr at 190C

a) Slow Tensile Fracture — 400X
b) Spall Fracture Surface — 400X
c) Slow Tensile Fracture — 4000X
d) Spall Fracture Surface — 4000X
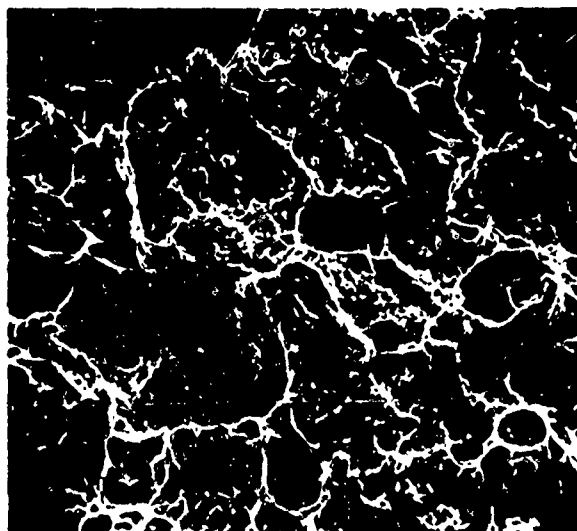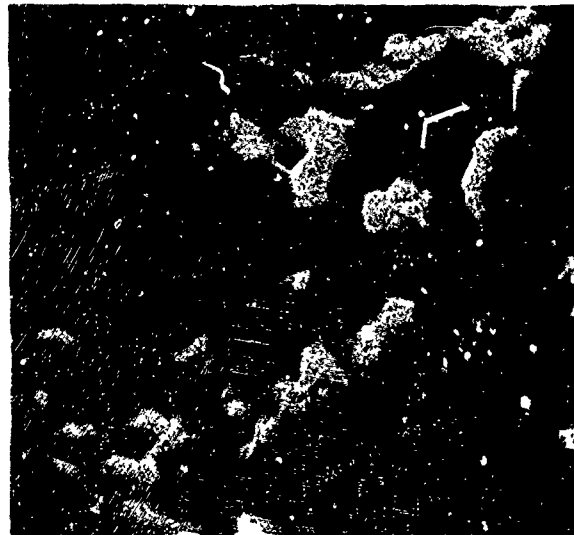
Figure 9. Scanning Electron Microscope Pictures of Fracture Surfaces
of Set II Material — Aged 12 Hr at 190C

a) Slow Tensile Fracture — 400X
b) Spall Fracture Surface — 400X
c) Slow Tensile Fracture — 4000X
d) Spall Fracture Surface — 4000X
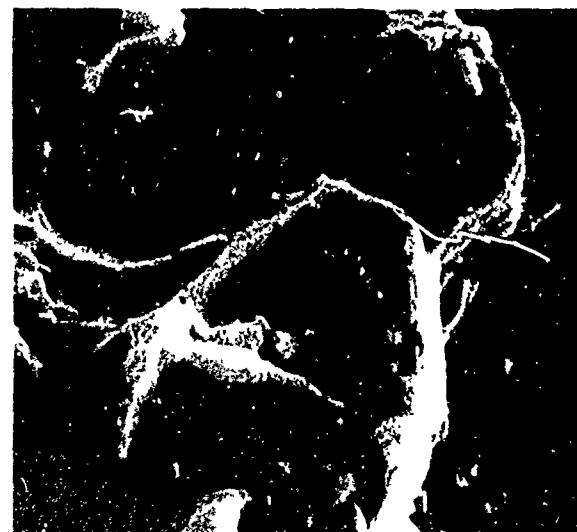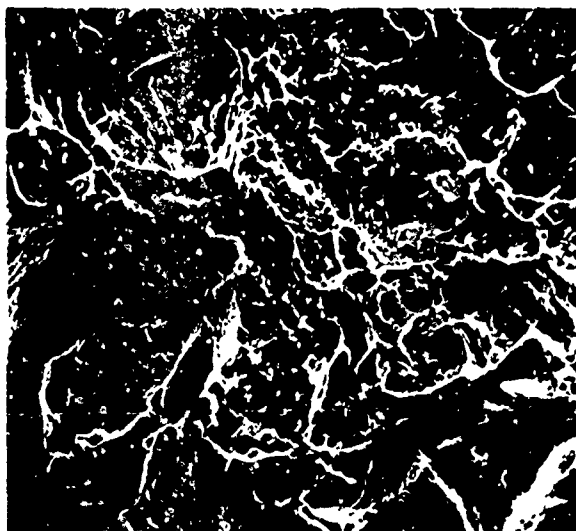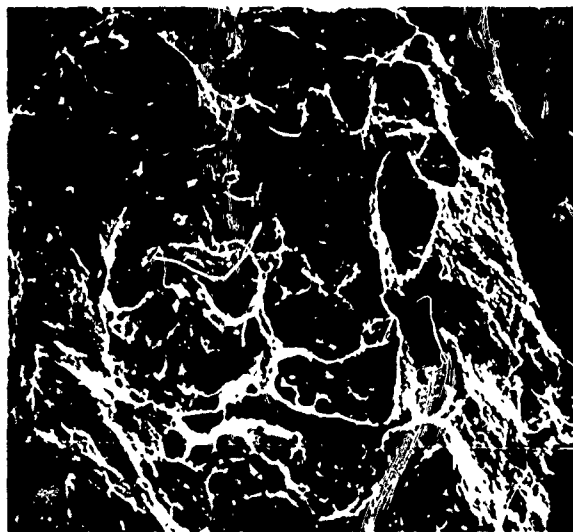
Figure 10. Scanning Electron Microscope Pictures of Fracture Surfaces
of Set III Materials    Aged 100 Hr at 190C

a) Slow Tensile Fracture — 400X
b) Spall Fracture Surface — 4000X
c) Slow Tensile Fracture — 4000X
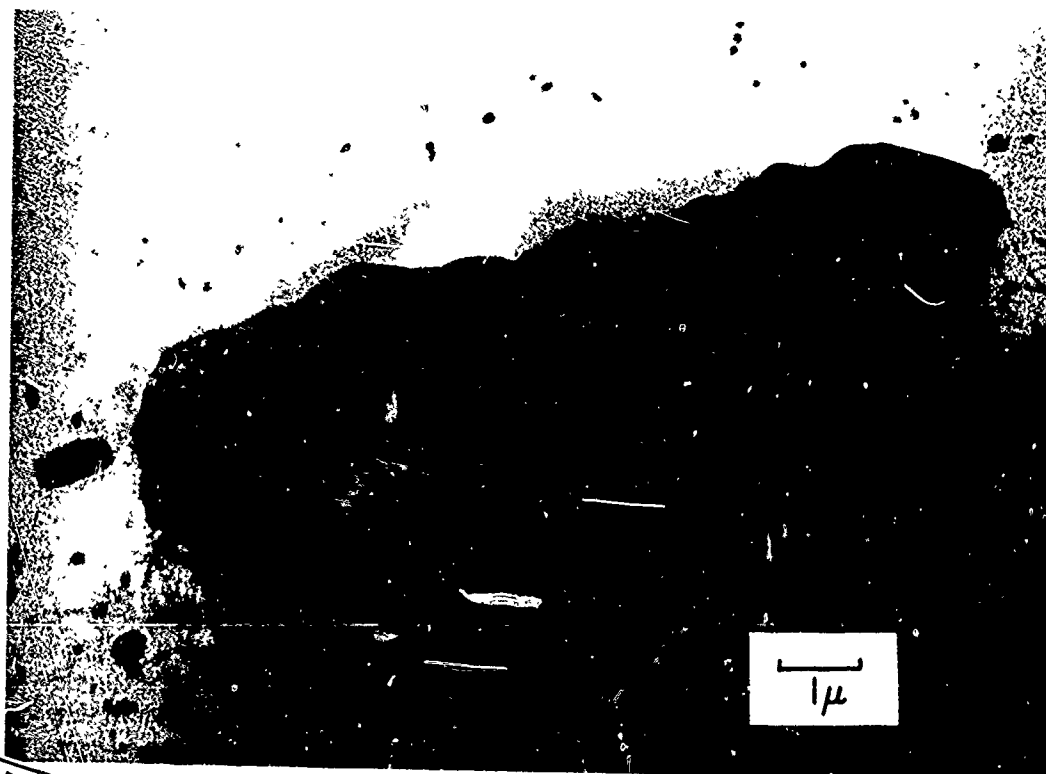d) Spall Fracture Surface — 4000X

Figure 11. Typical Large Inclusion Particle



Figure 12. Set I Material Cut Longitudinal to the Rolling Direction
Showing the Distribution of Dispersoid Particles and
Subgrain Structure

19

0.5 to 1.0µ. Those smaller, noncoherent particles, sometimes called disper-
soid particles, have been identified[11] as complex intermetallic compounds
containing aluminum, manganese, magnesium, iron, and silicon. In a high
purity Al-0.6% Mn alloy, they have been identified as $Al_6Mn$. The chief
function in the alloy of those dispersoid particles appears to be the control
of grain growth during the solution treatments which mainly affect the copper
rich precipitate phase.

The third class of precipitate present was the very fine Al-Cu-Mg
precipitate which is dissolved by the solution treatment and whose formation
and growth at the aging temperature gives rise to the aging characteristics
shown by the hardness curve in Figure 1.

Figure 13 shows a transverse section of unshocked set I material. In the
transverse section, the dispersoid particles elongated perpendicular to this
section appear more nearly equiaxed. The age hardening precipitate was not
resolved in set I material (aged one hour at 190C) but may contribute to the
speckling of the background in the figure.

Figure 14 shows an area of set I material from specimen I-5 impacted by
the mylar flyer plate at 2.3 mm/µsec. Extensive dislocation networks were
observed, especially in the region of inclusion particles such as the one in
the upper corner of Figure 14. The wave propagation direction, shown by the
arrow in Figure 14, was roughly perpendicular to the long axis of the large
inclusion particle. The dislocations appeared to form a braid or band structure
which can be seen fanning out from the end of the particle. Due to the
presence of the hardening precipitate and the dispersoid particles, disloca-
tions were not mobile enough to move under the influence of the heating
from the electron beam to provide surface slip traces. Without slip traces,
accurate foil thickness determinations are difficult and, hence, no attempt
to determine dislocation densities was made.

Figure 15 shows a transverse section of set II (peak hardness) material
in the unshocked condition. In that condition, the hardening precipitate
is resolved as two sets of fine parallel laths which appear almost at right
angles in this orientation. In Al-Cu-Mg alloys, the final aging product has
been identified as $Al_2CuMg$, commonly referred to as S phase, which has been
determined by Perlitz and Westgren[12] to be orthorhombic with lattice
parameters of a = 4.00, b = 9.23, and c = 7.14Å. The formation of the S phase
has been studied by Silcock[13] who reported the precipitation to occur by a
series of steps represented by

$$\text{Zones} \rightarrow \text{Zones} + S' \rightarrow S' + S \rightarrow S.$$
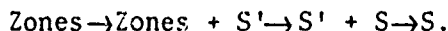
The zones which are present after the quench from the solution temperature
are reported to be cylindrical with a diameter of about 20Å and a length of
40 to 80Å, depending on the quench rate. These are aligned along $[100]_{Al}$
directions. On aging at 190C, Silcock concludes that the zones transform
to a coherent distorted form of the S phase which she calls S'. The peak
hardness was reported to occur when about a quarter of the S' had formed.

20

Figure 13. Set I Material Cut Transverse to the Rolling Direction.
The Al-Cu-Mg Hardening Precipitate is not Resolved
but Contributes the Speckled Background

Figure 14. Set I Material (Specimen I-5 Impacted at 2.3 mm/μ sec) —
A High Density Dislocation Structure Was Observed in the
Vicinity of Inclusions Such As the One Shown

Past the aging hardness peak, the conversion to S' is completed, and S' loses coherence and transforms to S phase as the hardness decreases at longer aging times. The S' phase shows a { 210 } habit plane. The kinetics of the growth of such laths in Al-Cu-Mg alloys has been studied by Sen and West. [14]

Figure 16 shows set III overaged material after impulse loading by the flyer plate at 2.5 mm/μsec. In addition to the S phase laths, a loosely defined dislocation cell structure is present with a cell size of approximately 1μ. Although no dislocation densities were measured, it appeared that the most dislocations were retained in shocked set I material.

## VI. Tensile Tests

The 0.2% yield strength, $\sigma_y$, the ultimate tensile strength, $\sigma_{uts}$, strain to fracture, $\epsilon_f$, ratio of the ultimate to yield stress, and the work hardening coefficient are tabulated in Table IV for the various aging times. From that data it can be seen that the yield strength is increased by aging up through 14 hours. The overaged condition at 100 hours, of course, shows a decrease of yield strength. The ultimate stress follows a similar trend with aging time but peaks earlier than does the yield stress. The work hardening coefficient decreased monotonically with aging. The strain to fracture went through a minimum at about the peak hardness condition, around 12 hours for this particular aging temperature.

Table IV - TRANSVERSE TENSILE PROPERTIES - 2024 ALUMINUM

| Aging Conditions | $\sigma_y$ (ksi) | $\sigma_{uts}$ (ksi) | $\dfrac{\sigma_{uts}}{\sigma_y}$ | K (ksi) | n | $\epsilon_f$ |
|---|---|---|---|---|---|---|
| Room Temp. only | 44.8 | 65.6 | 1.46 | 108 | 0.17 | 14% |
| 1 hr at 190C | 42.9 | 63.5 | 1.48 | 108 | 0.19 | 14% |
| 9 hrs at 190C | 57.7 | 68.4 | 1.18 | 95 | 0.10 | 5% |
| 14 hrs at 190C | 60.1 | 67.2 | 1.12 | 95 | 0.09 | 5% |
| 100 hrs at 190C | 46.2 | 56.3 | 1.22 | 74 | 0.07 | 9% |

## DISCUSSION

The most notable result of this study is that the aged condition does influence the incipient spall threshold of otherwise identical material. Set I, the underaged material, displayed higher resistance to internal spall cracking, as judged from surface observations in Figures 2, 3, and 4 and on the basis of metallographic observation of polished sections. While the differences are not great, set I does appear to have an incipient spall threshold 10 to 15% above that of the peak hardness, set II, or of the overaged, set III, material.

Figure 15. Set II Material  Unshocked — After 12 Hr Aging at 190C, the Hardening Percipitate is Resolved as Sets of Fine Parallel Laths
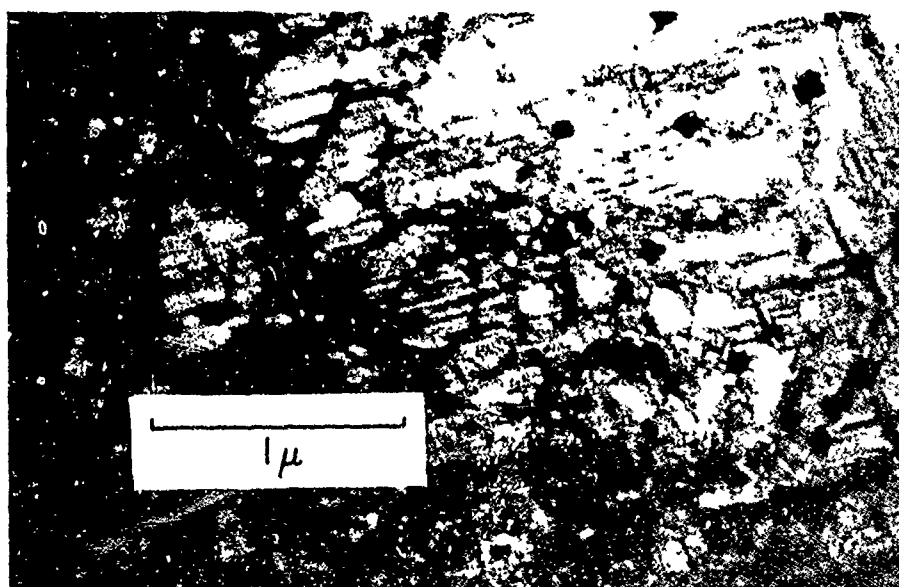


Figure 16. Set III Material (Specimen III-5 Impacted at 2 3 mm/μ sec) — Moderate Density Dislocation Nets Form a Loose Cell Structure

23

The set III material had least resistance to tearing away of the spall material as shown by the complete separation of material from the rear surface of specimen III-8. Figure 5 also shows that the deformation of the material is greatest in set III for comparable impact velocities.

Once the separation has occurred internally in the specimen, the detached layer (constrained at its edges where separation is prevented by edge effects) will bulge outward. It will continue to bulge until the energy trapped in that layer has been expended in deforming the spall layer. In the plate geometry used for these tests, a detailed analysis of the bulging of that spall layer would be complicated due to the simultaneous biaxial stretching of the spall layer and bending at its edges. However, the lower work hardening coefficient (n = 0.07) found in the tensile tests for set III material may be related to the larger separation of the spall layer at comparable impact velocities, as shown by the composite of sections in Figure 5.

The general trend of the shock hardening, being greatest for set I material and least for set III material, also reflects the work hardening ability of the material and follows the trend found in the uniaxial tensile tests in which the work hardening coefficient decreased monotonically with aging time. The shock hardening shown by Figure 7 was greatest on the impacted side of the specimens and decayed with distance in much the same way the elastic precursor wave has been noted to attenuate.[15] Analyses of precursor wave attenuation in terms of a dislocation velocity relation have been given by Taylor[16] and others.[17,18] In those treatments, dislocation motion, under the action of the shear stresses of the precursor wave, attenuate that wave, and the precursor should leave behind the high dislocation densities seen in transmission electron microscopy studies such as shown by Figures 14 or 16. Those dislocations contribute to the increase in hardness detected by the microhardness results shown in Figure 7. If the work hardening coefficient measured in a uniaxial tensile test is a reflection of the ability of the internal structure to build up a high dislocation density structure, the measurements of n should and do correlate with the shock hardening ability observed, as well as the qualitative observation of higher density and more uniform dislocation structures in set I material.

Tuler[19] has compared scanning electron micrographs of slow bend fracture and spall fracture surfaces to demonstrate that strain rate has very little influence on fracture appearance in 6061-T6 aluminum. The results presented here show that the same is true for peak hardness and overaged 2024 aluminum. The results for the underaged alloy, however, demonstrate that extreme strain rate can have a pronounced effect on fracture appearance. The fracture mode was changed from normal ductile void coalescence to a less ductile mode dominated by the larger inclusions. This indicates that the role of the inclusions in failure is increased at the higher strain rate. Elimination of these inclusions would, therefore, be expected to increase the incipient spall threshold of the material. Since the aging treatment influences only the fine structure of the material, the observation that all the spall fracture surfaces were dominated by inclusions suggests that the effect of aging was somewhat masked by the presence of the inclusions, the only aging effect being

24

the suggestion of fewer fine cusps in the underaged material. The masking effect of the inclusions would also be true for mechanical properties. A similar study using high purity materials might better define the role of aging treatment on the spall behavior of these alloys.

## CONCLUSIONS

1.   The precipitation state in an age hardenable material has been shown to influence the incipient spall threshold of the material. About 10 to 15% higher incipient spall thresholds were noted for underaged material compared with peak hardness or overaged material.

2.   The work hardening coefficient, as measured in uniaxial tensile tests, correlated with the ability of the material to harden due to propagation of an impulsive wave through the material. Both the work hardening coefficient and shock hardening were greatest for the underaged (set I) material and were least in the overaged (set III) material.

3.   The high strain rate was observed to change the fracture mode of the underaged (set I) material to a less ductile mode dominated by inclusion particles. The peak hardness and overaged (sets II and III) material showed no influence of strain rate on fracture appearance, since the less ductile mode (inclusion particles) was also exhibited in the slow tensile test. It is expected that elimination of the inclusions would substantially increase the incipient spall threshold of these materials.

## ACKNOWLEDGMENTS

## LITERATURE CITED

1. Butcher, B.M., Berker, L.M., Munson, D.E. and Lundergan, C.D. AIAA Journal, $\underline{2}$(1964), P. 977.

2. Tuler, F.R. and Butcher, B.M. Intl. J. of Frac. Mech., $\underline{4}$(1968), p. 431.

3. Rinehart, J.S. and Pearson, J. Behavior of Metals Under Impulsive Loads, Dover, 1965.

4. Cohen, L.J. and Berkowitz, H.M. AFML TR-69-106 Parts 1, II, and III.

5. Metals Handbook - 8th Edition, Vol. 1, ASM, 1961, p. 938.

6. Kohn, B.J. AFWL TR-69-38.

7. Rice, M.H., McQueen R.G. and Walsh, J.M., in Solid State Physics, F. Seitz and D. Turnbull, eds., Vol. 6, Academic Press, 1958, pp. 1-63.

8. Mechanical Behavior of Materials Under Dynamic Loads, U.S. Lindholm, ed., Springer-Verlag, 1968.

9. Kelly, P.M. and Nutting, J. J. Inst. of Metals, $\underline{87}$ (1959), p 385.

10. Nunes, J. and Larson, F.R. WAL TR-111.1/1, March 1961.

11. Grosskreutz, J.R. and Shaw, G.G., in Fracture-1969: Proc. 2nd Intl. Conf. on Fracture, Chapman and Hall, 1969.

12. Perlitz, H. and Westgren, A. Arkiv Kemi, Min. Geol., $\underline{B16}$, (1943), p 13.

13. Silcock, J.M. J. Inst. of Metals, $\underline{89}$ (1960), p 203.

14. Sen, N. and West, D.F.R. J. Inst. of Metals, $\underline{97}$ (1969), p 87.

15. Taylor, J.W. and Rice, M.H. J Appl. Phys., $\underline{34}$ (1963), p 364.

16. Taylor, J.W. J. Appl. Phys., $\underline{36}$ (1965), p 3146.

17. Kelly, J.M. and Gillis, P.P. J. Appl. Phys., $\underline{38}$ (1967).

18. Butcher, B.M. and Munson, D.E., in Dislocation Dynamics, ed. A.R. Rosenfield et al., McGraw-Hill (1968), p 591.

19. Tuler, F.R. Sandia Laboratories Development Report SC-DR-68-497, Oct., 1968.

26

APPENDIX

IMPACT LOADING CONDITIONS

The following is a condensation of a memorandum which reported the experimental conditions and the optical data for the flyer plate velocities used in the tests conducted on the 2024 aluminum samples.

University of Dayton
Research Institute

To:        H.F. Swift                                                    March 17, 1970

From:      P.W. Dueweke

Subject:   Damage Study of 7075 and 2024 Aluminum

A study of the failure threshold of 7075 and 2024 aluminum was conducted under one-dimensional dynamic loading conditions. The 7075 series consisted of two different hardnesses, T0 and T6, tested with two different edge support techniques, steel shock block supports and free surface supports. The steel shock block supports were made up of four 0.25 x 0.25 x 1.25 in. steel blocks in intimate contact with the target edges (thin vacuum grease interface) and held in place by winding with tape. The free surface supports consisted of heavy bonds of low acoustical impedance rubber adhesive holding the target to the vacuum chamber walls. The 2024 series consisted of three sets of six 2.0 x 2.0 x 0.25 in. samples, each set representing a different precision heat treating process. Two of the samples from each set were cut into eight 1.0 x 1.0 in. pieces. The other four samples in each set were cut down to 1.4 x 1.4 in. pieces. All of the cutting was done cold so that the heat treatments would be preserved. The free surface support technique was used exclusively with the 2024 series. In each test a 1.5 x 1.5 x 0.005 in. Mylar sheet was launched in a reduced pressure environment of between 5 and 80 microns.

Thus seven separate series were run and the following tables present the results. Planarities were measured parallel to the target front surface between the first and the last points of contact between the flyer and the target. This distance was then converted to a time between first and last contact using the flyer velocity.

The damage level assigned to each target is a rather subjective and qualitative description of visable spall damage. Incipient spall is the bulging of the separated spall layer without it becoming detached from the rest of the target. Spall means that the spall layer has become completely detached.

One conclusion which can be drawn from the 7075 tabulated data is that there is no difference among the four groups in the level at which visable damage becomes apparent on the rear surface. This level is approximately

2200 taps. However, heavy spall for the T6 with free surface support begins
between 3900 and 4300 taps while this damage does not begin until somewhere
above 4700 taps for the T6 with shock block supports. Thus the shock block
supports seem to reduce the rear surface peak pressure at high impulse levels,
i.e., they seem to provide more resistance to heavy spall than to lower
damage levels. However, no such dissimilar behavior exists for the T0. In
fact very good agreement exists between the high impulse level damage in T0
with shock block supports and T0 with free surface supports.

Within the uncertainty indicated by the tables the visible damage thresh-
olds of both the 2024-II and 2024-III are approximately the same, i.e., 1800-
2000 taps. The threshold of 2024-I is higher at about 2200-2300 taps.

Little more can be said about damage-impulse correlations until a quanti-
tative damage analysis can be performed on both the microscopic and macro-
scopic scale using dissection, acoustical reflection, X-ray, or some other
analytical techniques.

The density of each type of 7075 aluminum was determined from measure-
ments of sample dimensions and mass. Values of 2.7788 g/cm$^3$ ($\sigma = 0.0030$ g/cm$^3$)
and 2.7774 g/cm$^3$ ($\sigma = 0.0057$ g/cm$^3$) were measured for representative groups
of the 7075-T0 and T6 samples, respectively. The sound speed was also measured
to be 6.059 mm/$\mu$sec and 6.133 mm/ sec ($+\sim 5\%$ estimated) for the T0 and T6
samples, respectively. The density of the 2024 aluminum was not measured;
however, its sound speed was measured to be 6.44 mm/$\mu$sec.

## Table I - 2024-I ALUMINUM

| Shot No. | Area (in$^2$) | Voltage (kV) | Velocity (mm/$\mu$sec) | Momentum (Taps) | Planarity ($\mu$sec) | Thickness (mm) |
|---|---|---|---|---|---|---|
| 5316 | 2 | 5.89 | 1.107 + 0.021 | 1927 + 36 | 1.155 | 6.32 |
| 5315 | 2 | 6.32 | 1.241 + 0.020 | 2159 + 34 | 0.614 | 6.36 |
| 5314 | 2 | 7.06 | 1.339 + 0.026 | 2330 + 46 | 0.668 | 6.35 |
| 5305 | 1 | 9.02 | 1.7 + 0.1* | 2960 + 170 | | 6.37 |
| 5306 | 1 | 10.14 | 1.712 + 0.085 | 2980 + 148 | 0.366 | 6.37 |
| 5311 | 1 | 9.64 | 1.723 + 0.038 | 2998 + 65 | 0.356 | 6.33 |
| 5313 | 2 | 11.08 | 1.806 + 0.046 | 3143 + 80 | 0.332 | 6.29 |
| 5310 | 1 | 10** | 1.9 + 0.1* | 3210 + 170 | | 6.33 |
| 5312 | 1 | 13.40 | 2.319 + 0.088 | 4035 + 153 | 0.224 | 6.33 |
| 5308 | 1 | 18.07 | 2.6 + 0.2* | 4530 + 350 | | 6.37 |
| 5307 | 1 | 15.96 | 2.672 + 0.057 | 4650 + 99 | 0.295 | 6.36 |
| 5309 | 1 | 19.92 | 2.986 + 0.053 | 5196 + 92 | 0.525 | 6.33 |

*Insufficient optical data to determine velocity. This is an estimate.
**Capacitor bank fired before desired voltage was attained.

## Table II - 2024-II ALUMINUM

| Shot No. | Area (in$^2$) | Voltage (kV) | Velocity (mm/µsec) | Momentum (Taps) | Planarity (µsec) | Thickness (mm) |
|---|---|---|---|---|---|---|
| 5332 | 2 | 5.48 | 0.467 ± 0.011* | 812 ± 20 | 3.278 | 6.35 |
| 5317 | 2 | 5.80 | 0.966 ± 0.050 | 1680 ± 87 | 0.832 | 6.29 |
| 5330 | 1 | 6.51 | 1.170 ± 0.102 | 2036 ± 177 | 0.873 | 6.38 |
| 5333 | 2 | 7.04 | 1.174 ± 0.059 | 2043 ± 103 | 0.354 | 6.36 |
| 5329 | 1 | 8.14 | 1.286 ± 0.059 | 2237 ± 102 | 0.685 | 6.37 |
| 5328 | 1 | 8.12 | 1.5 ± 0.1** | 2610 ± 170 |  | 6.37 |
| 5331 | 2 | 9.00 | 1.953 ± 0.063 | 3399 ± 110 | 0.467 | 6.35 |
| 5320 | 1 | 10.04 | 1.955 ± 0.405 | 3401 ± 705 | 0.450 | 6.30 |
| 5319 | 1 | 11.02 | 1.971 ± 0.042 | 3430 ± 72 | 0.187 | 6.30 |
| 5321 | 1 | 12.13 | 2.189 ± 0.021 | 3809 ± 37 | 0.227 | 6.31 |
| 5327 | 1 | 16.07 | 2.452 ± 0.051 | 4266 ± 89 | 0.187 | 6.37 |
| 5322 | 1 | 20.00 | 2.841 ± 0.153 | 4943 ± 266 | 0.317 | 6.30 |

*Flyer not completely sheared out.
**Insufficient optical data to determine velocity. This is an estimate.

## Table III - 2024-III ALUMINUM

| Shot No. | Area (in$^2$) | Voltage (kV) | Velocity (mm/µsec) | Momentum (Taps) | Planarity (µsec) | Thickness (mm) |
|---|---|---|---|---|---|---|
| 5340 | 2 | 5.65 | 0.690 ± 0.021 | 1201 ± 37 | 2.040 | 6.35 |
| 5318 | 2 | 5.79 | 1.036 ± 0.023 | 1804 ± 40 | 1.765 | 6.35 |
| 5339 | 2 | 7.02 | 1.292 ± 0.041 | 2248 ± 71 | 0.866 | 6.39 |
| 5326 | 1 | 6.47 | 1.374 ± 0.035 | 2391 ± 60 | 0.939 | 6.35 |
| 5337 | 1 | 8.03 | 1.5 ± 0.1* | 2610 ± 170 |  | 6.37 |
| 5338 | 2 | 9.06 | 1.859 ± 0.044 | 3234 ± 77 | 0.273 | 6.33 |
| 5335 | 1 | 10.00 | 1.9 ± 0.1* | 3300 ± 170 |  | 6.37 |
| 5336 | 1 | 11.01 | 1.992 ± 0.126 | 3466 ± 220 | 0.325 | 6.37 |
| 5323 | 1 | 11.95 | 2.292 ± 0.051 | 3988 ± 88 | 0.437 | 6.35 |
| 5325 | 1 | 16.00 | 2.491 ± 0.042 | 4334 ± 73 | 0.391 | 6.35 |
| 5334 | 1 | 16.06 | 2.532 ± 0.078 | 4406 ± 136 | 0.281 | 6.37 |
| 5324 | 1 | 20.02 | 2.650 ± 0.072 | 4612 ± 125 | 0.581 | 6.35 |

*Insufficient optical data to determine velocity. This is an estimate.